arXiv:1404.1662v2 [cond-mat.supr-con] 5 Nov 2014

Non-magnetic impurity effects in a three-dimensional topological superconductor: From p- to s-wave behaviors

Yuki Nagai,[1] Yukihiro Ota,[1] and Masahiko Machida[1]

[1] *CCSE, Japan Atomic Energy Agency, 5-1-5 Kashiwanoha, Kashiwa, Chiba 277-8587, Japan*

(Dated: November 6, 2014)

Unconventional features in superconductivity are revealed by responses to impurity scattering. We study non-magnetic impurity effects in a three-dimensional topological superconductor, focusing on an effective model (massive Dirac Hamiltonian with s-wave on-site pairing) of Copper-doped bismuth-selenium compounds. Using a self-consistent T-matrix approach for impurity scattering, we examine in-gap states in density of states. We find that the results are well characterized by a single material variable, which measures relativistic effects in the Dirac Hamiltonian. In non-relativistic regime, an odd-parity superconducting state is fragile against non-magnetic impurities. We show that this behavior is caused by a p-wave character involved in the topological superconducting state. In contrast, we show that in relativistic regime the superconductivity is robust against non-magnetic impurities, owing to an s-wave character. To summarize, the system has two aspects, p- and s-wave features, depending on the weight of relativistic effects.

PACS numbers: 74.20.Rp,74.25.-q,74.90.+n

I. INTRODUCTION

Topological materials[1–5] are attracting a great deal of attention in condensed matter physics. The seminal studies[6–9] indicate that a superconducting state can emerge, with topological invariants, such as the Thouless-Kohmoto-Nightingale-Nijs invariant[10] and the Kane-Mele Z_2 invariant.[11,12] Topological superconductivity is predicted in both two- and three-dimensional systems. Copper-doped bismuth-selenium compounds[13,14] are candidates for bulk topological superconductors, and their properties are studied by different physical probes, including point-contact spectroscopy,[15,16] magnetization curve,[17] and scanning tunneling spectroscopy.[18] Among them, the zero-bias conductance peaks with point-contact spectroscopy[15,16] can be strong evidence for the topological superconductivity, although identifying the gap-function type is an unsettled issue; the scanning tunneling spectroscopy measurement[18] shows that in $Cu_{0.2}Bi_2Se_3$ the density of states (DOS) at the Fermi level is a fully-gapped behavior, leading to a conventional (presumably, non-topological) superconducting state. Furthermore, the study about topological superconductors includes different physical areas, such as color superconductivity in quark matter.[19]

Impurity effects are typically studied for examining unconventional properties of superconductivity.[20–24] Assessing the impurity effects of topological superconductors is desirable for not only finding the unconventional features, but also developing a theory of nano-scale devices composed of these materials. The authors[25] studied the impurity effects in a two-dimensional topological superconductor with the Zeeman term.[9] Remarkably, the superconducting transition temperature for a certain magnetic-field domain is significantly affected by non-magnetic impurities, although the pair potential has an isotropic s-wave character. The reduction of T_c is linked with the occurrence of surface edge modes. This result arises a question. Do non-magnetic impurities diminish the superconductivity in other models, especially systems with time-reversal symmetry?

In this paper, we study the impurity effects in a three-dimensional topological superconductor, with time-reversal symmetry and s-wave on-site pairing. Using a mean-field Hamiltonian and a self-consistent T-matrix approach for impurity scattering, we calculate the DOS and examine the presence of in-gap states, with two kinds of fully-gapped states, i.e., an even-parity state and an odd-parity one. We find that all the results are summarized well by a single material variable. This variable characterizes *relativistic* effects in the Dirac Hamiltonian for normal part of this model. When the system is in non-relativistic regime, the odd-parity state is suffered from non-magnetic impurities. In contrast, in relativistic regime, no low-energy excitation is induced by non-magnetic impurity; the topological superconductivity is robust against non-magnetic impurities. To understand these behaviors, we derive an effective Hamiltonian in two limiting cases. In the non-relativistic limit, the effective Hamiltonian for the odd-parity gap function describes p-wave superconductivity. Since the Anderson's theorem is violated for p-wave symmetry, the non-magnetic impurities induce low-energy in-gap states, and as a result the superconducting state is fragile. In the ultra-relativistic limit, the effective Hamiltonian is the same as the s-wave mean-field Hamiltonian, irrespective of the gap-function types. In contrast to the non-relativistic limit, the Anderson's theorem leads to the protection of the superconductivity from non-magnetic impurities. To sum up, the full-gap states in this topological superconductor have two aspects, p- and s-wave characters, depending on the weight of relativistic effects in the normal-state Dirac Hamiltonian.

The paper is organized as follows. Section II shows the model and our approach for impurity scattering in super-

conductivity. We also define an indicator of relativistic effects. Section III is main part of this paper. We show the DOS for two different gap functions, either even parity or odd parity, changing the indicator of relativistic effects. The results are concisely summarized in Table I. Section IV is devoted to summary.

II. FORMULATION

A. Model

We study a model of a topological superconductor in a three-dimensional system, with mean-field approximation. Typically, this model is used for examining Copper-doped Bi_2Se_3 in literature[7,15,26–32]. The parent compound is considered to be a three-dimensional strong topological insulator. The notable feature is the band structure around the Γ point[34]. The effective Hamiltonian with a strong spin-orbit coupling around Γ point is equivalent to that of the massive Dirac Hamiltonian with the negative Wilson mass term. This negative term creates an insulator with a topological twist, in terms of the Kane-Mele Z_2 invariant[11]. A low-energy effective theory of $Cu_xBi_2Se_3$ is derived, with the chemical potential located in the conduction band.[7,15,26]

The mean-field Hamiltonian is

$$H = \frac{1}{2}\sum_{\boldsymbol{k}} \boldsymbol{\Psi}_{\boldsymbol{k}}^{\dagger}\mathcal{H}(\boldsymbol{k})\boldsymbol{\Psi}_{\boldsymbol{k}}. \tag{1}$$

The 8-component column vector $\boldsymbol{\Psi}_{\boldsymbol{k}}$ has the electron annihilation operators $c_{\boldsymbol{k},\alpha,s}$ in the upper 4-component block (particle space) and the electron creation operators $c^{\dagger}_{-\boldsymbol{k},\alpha,s}$ in the lower 4-component block (hole space), with momentum $\boldsymbol{k}$, orbital α (= 1, 2), and spin s (=↑, ↓). The arrangement of the upper 4-component block is ${}^{\mathrm{t}}(c_{\boldsymbol{k},1,\uparrow}, c_{\boldsymbol{k},1,\downarrow}, c_{\boldsymbol{k},2,\uparrow}, c_{\boldsymbol{k},2,\downarrow})$. The lower one is written in a similar manner. The Bogoliubov-de Gennes (BdG) Hamiltonian[15,26] is an 8×8 hermitian matrix,

$$\mathcal{H}(\boldsymbol{k}) = \begin{pmatrix} h_0(\boldsymbol{k}) & \Delta_{\mathrm{pair}}(\boldsymbol{k}) \\ \Delta_{\mathrm{pair}}^{\dagger}(\boldsymbol{k}) & -h_0^{*}(-\boldsymbol{k}) \end{pmatrix}, \tag{2}$$

with the normal-state Hamiltonian

$$h_0(\boldsymbol{k}) = \varepsilon(\boldsymbol{k}) + d_0(\boldsymbol{k})\gamma^0 + \sum_{i=1}^{3} d_i(\boldsymbol{k})\gamma^0\gamma^i, \tag{3}$$

and the 4×4 pairing potential matrix Δ_{pair}. The 4×4 complex matrices γ^{μ} (μ = 0, 1, 2, 3) are the Gamma matrices in the Dirac basis[35]. Using the orbital 2×2 Pauli matrices σ^i and the spin 2×2 Pauli matrices s^i, we have $\gamma^0 = \sigma^3\otimes \mathbb{1}_2$ and $\gamma^i = i\sigma^2\otimes s^i$.

We summarize the properties of the normal part h_0 and the superconducting part Δ_{pair} in the BdG Hamiltonian. First, we focus on the normal part. We use the following formulae[15]. For the diagonal block, we have $\varepsilon = -\mu + \bar{D}_1\epsilon_c(\boldsymbol{k}) + (4/3)\bar{D}_2\epsilon_{\perp}(\boldsymbol{k})$ and $d_0 = M_0 - \bar{B}_1\epsilon_c(\boldsymbol{k}) - (4/3)\bar{B}_2\epsilon_{\perp}(\boldsymbol{k})$, with $\epsilon_c = 2 - 2\cos(k_z)$, $\epsilon_{\perp} = 3 - 2\cos(\sqrt{3}k_x/2)\cos(k_y/2) - \cos(k_y)$. The off-diagonal block has contributions from the spin-orbit couplings, $d_1 = (2/3)\bar{A}_2\sqrt{3}\sin(\sqrt{3}k_x/2)\cos(k_y/2)$, $d_2 = (2/3)\bar{A}_2[\cos(\sqrt{3}k_x/2)\sin(k_y/2) + \sin(k_y)]$, and $d_3 = \bar{A}_1\sin(k_z)$. The material parameters ($\bar{D}_1$, $\bar{D}_2$, M_0, $\bar{B}_1$, $\bar{B}_2$, $\bar{A}_2$, $\bar{A}_1$) and the chemical potential μ will be set, in a manner compatible with literature.[15]

Next, we turn into the pairing potential Δ_{pair}. This 4×4 matrix must fulfill the relation ${}^{\mathrm{t}}\Delta_{\mathrm{pair}}(-\boldsymbol{k}) = -\Delta_{\mathrm{pair}}(\boldsymbol{k})$, owing to the fermionic property of $c_{\boldsymbol{k},\alpha,s}$ and $c^{\dagger}_{\boldsymbol{k},\alpha,s}$.[36] In this paper, we study the case when Δ_{pair} has no dependence on $\boldsymbol{k}$. Using the above two properties, we have six possible superconducting classes.[26] They are classified by a Lorentz-transformation property.[28,30,31,33] To see this point, we expand $\Delta_{\mathrm{pair}}i\gamma^2$ by a complete orthogonal system (a set of sixteen complex matrices) built up by the Gamma matrices and the identity.[35] A straightforward calculation leads to

$$\Delta_{\mathrm{pair}}i\gamma^2 = i\gamma^0\left(f^{\mathrm{s}} + f^{\mathrm{ps}}\gamma^5 + \sum_{\mu=0}^{3} f_{\mu}^{\mathrm{pv}}\gamma^{\mu}\right)\gamma^5, \tag{4}$$

with $\gamma^5 = i\gamma^0\gamma^1\gamma^2\gamma^3$. The possible non-zero coefficients are related to a scalar (f^{s}), a pseudo scalar (f^{ps}), and a polar vector (f_{μ}^{pv}). Since the spatial inversion in this system[8,37] is defined by $\mathcal{P} = \sigma^3\otimes\mathbb{1}_2 = \gamma^0$ and transforms Δ_{pair} into $\mathcal{P}^{\dagger}\Delta_{\mathrm{pair}}\mathcal{P}^{*}$, the parity of the six superconducting gaps[7,8] is described by $f^{\mathrm{ps}} \to -f^{\mathrm{ps}}$, $f_i^{\mathrm{pv}} \to -f_i^{\mathrm{pv}}$, $f^{\mathrm{s}} \to f^{\mathrm{s}}$, and $f_0^{\mathrm{pv}} \to f_0^{\mathrm{pv}}$. Therefore, the odd-parity superconductivity emerges when either f^{ps} or f_i^{pv} are not zero, and the others vanish. This superconducting order is characterized topologically.[7,8] using an analogy with the Z_2 invariant for topological insulators with spatial inversion symmetry.[12]

B. Indicator of relativistic effects

We show a primary variable in this paper, to characterize the impurity effects in the present model. Let us examine normal-state part h_0 closely. We find that the mass M_0 and the spin-orbit couplings ($\bar{A}_2$ and $\bar{A}_1$) are related to a low-energy behavior of h_0. Taking $|\boldsymbol{k}| \to 0$, we find that h_0 corresponds to the massive Dirac equation with anisotropy along the z-axis,

$$h_0 \approx -\mu + \gamma^0[M_0 + \bar{A}_2(k_x\gamma^1 + k_y\gamma^2) + \bar{A}_1k_z\gamma^3] + \mathcal{O}(|\boldsymbol{k}|^2). \tag{5}$$

Therefore, we may define an indicator of relativistic effects in h_0 as[38]

$$\beta = \frac{\bar{A}_2k_F}{|M_0|}, \tag{6}$$

with $\bar{A}_2 k_F = \sqrt{\mu^2 - M_0^2}$. The Dirac Hamiltonian has two distinct behaviors, depending on β; a non-relativistic limit ($\beta \to 0$, i.e., a large-mass limit) and a ultra-relativistic limit ($\beta \to \infty$, i.e., a massless limit). This variable plays a central role for understanding the impurity effects.

C. Formalism for impurity scattering: Self-consistent T-matrix approach

The effects of impurity scattering are taken as self-energy, with the self-consistent T-matrix approximation. We consider the randomly distributed non-magnetic (magnetic) impurity potentials [e.g., $V(\boldsymbol{r}) = \sum_i \delta(\boldsymbol{r} - \boldsymbol{r}_i) V^{\rm NM(M)}$]. The T-matrix for randomly distributed non-magnetic (magnetic) impurities[39] is

$$T(\Omega) = \left[1 - V^{\rm NM(M)} \frac{1}{N} \sum_{\boldsymbol{k}} G_{\boldsymbol{k}}(\Omega) \right]^{-1} V^{\rm NM(M)}, \quad (7)$$

with

$$V^{\rm NM} = V_0 \begin{pmatrix} \mathbb{1}_2 \otimes \mathbb{1}_2 & 0 \\ 0 & -\mathbb{1}_2 \otimes \mathbb{1}_2 \end{pmatrix}, \quad (8)$$

$$V^{\rm M} = V_0 \begin{pmatrix} \mathbb{1}_2 \otimes s^3 & 0 \\ 0 & -\mathbb{1}_2 \otimes s^3 \end{pmatrix}, \quad (9)$$

where N is the number of meshes in momentum space. The Green's function is

$$G_{\boldsymbol{k}}(\Omega) = \frac{1}{\Omega - \mathcal{H}(\boldsymbol{k}) - \Sigma(\Omega)} = \begin{pmatrix} g_{\boldsymbol{k}}(\Omega) & f_{\boldsymbol{k}}(\Omega) \\ f^\dagger_{\boldsymbol{k}}(\Omega) & \bar{g}_{\boldsymbol{k}}(\Omega) \end{pmatrix}, \quad (10)$$

with the self-energy

$$\Sigma(\Omega) = n_{\rm imp} T(\Omega) - n_{\rm imp} V^{\rm NM(M)}. \quad (11)$$

The impurity concentration is written by $n_{\rm imp}$. The second term in Eq. (11) corresponds to the renormalization of the chemical potential μ, since in our calculations μ is fixed. If one self-consistently calculates μ with fixed particle number, this term is not needed. Solving Eqs. (7), (10), and (11) self-consistently, we obtain the density of states (DOS)

$$N(E) = -\frac{1}{2\pi} \frac{1}{N} \sum_{\boldsymbol{k}} {\rm tr}\, [{\rm Im}\, g_{\boldsymbol{k}}(E)], \quad (12)$$

with given μ and gap amplitude Δ. We will examine the impurity effects in topological superconductivity, via the energy dependence of the DOS. We can find that the main results do not change, when performing the full self-consistent calculations (i.e., the T-matrix formula with the gap equation).

III. RESULTS

We study the impurity effects of both even- and odd-parity gaps, checking in-gap states at low-energy (less than gap amplitude) region in the DOS. All the results are summarized in Table I. For even parity, we focus on the scalar gap, $f^{\rm s}$. Using the notations in Sasaki *et al.*,[15] we find that $\Delta^{11}_{\uparrow\downarrow} = -\Delta^{11}_{\downarrow\uparrow}$, $\Delta^{22}_{\uparrow\downarrow} = -\Delta^{22}_{\downarrow\uparrow}$, $\Delta^{11}_{\uparrow\downarrow} = \Delta^{22}_{\uparrow\downarrow}$, and the other components of the pairing potential matrix are zero. The gap amplitude is $\Delta = |f^{\rm s}| = |\Delta^{11}_{\uparrow\downarrow}|$. In terms of Hao and Lee,[26] this state correspond to even-parity intra-orbital singlet pairing. For odd parity, we study the pseudo-scalar gap, $f^{\rm ps}$. In a similar manner to $f^{\rm s}$, we find that $\Delta^{12}_{\uparrow\downarrow} = -\Delta^{12}_{\downarrow\uparrow}$, $\Delta^{21}_{\uparrow\downarrow} = -\Delta^{21}_{\downarrow\uparrow}$, $\Delta^{12}_{\uparrow\downarrow} = \Delta^{21}_{\uparrow\downarrow}$, and the others are zero. The gap amplitude in this case is $\Delta = |f^{\rm ps}| = |\Delta^{12}_{\uparrow\downarrow}|$. Both $f^{\rm s}$ and $f^{\rm ps}$ have a full-gap feature in their spectral functions.[15]

Let us summarize the parameter sets for numerically calculating the DOS in this paper. The $\boldsymbol{k}$-mesh size is $256 \times 256 \times 256$. We focus on a unitary-like scattering model with $V_0 = 10\,{\rm eV}$ and $n_{\rm imp} = 0.005$, to study a case that the superconducting pair is broken drastically. The gap amplitude is $\Delta = 0.1\,{\rm eV}$ for both even- and odd-parity superconducting states. The material parameters for most of the calculations are set by $(\bar{D}_1, \bar{D}_2, \bar{B}_1, \bar{B}_2, \bar{A}_1, \bar{A}_2) = (0, 0, -0.5, -0.75, 1, 1.5)$, in unit of eV. When we choose different values, we will show them explicitly. The unit of energy is eV throughout this paper, unless otherwise noted. These parameters are the same as the ones in Ref. 15. In the subsequent parts, the relativity indicator β is tuned, changing M_0 with $|\mu| - |M_0| = 0.2\,{\rm eV}$. This difference is the same value as in Ref. 15.

A. Scalar gap (non-topological superconductivity)

We study the impurity effects of the scalar gap $f^{\rm s}$ (even parity). We set $M_0 = -0.6\,{\rm eV}$ and $\mu = 0.8\,{\rm eV}$ (i.e., $\beta \sim 0.88$). Figure 1 shows that the non-magnetic impurities (green square) do not induce in-gap states. This result corresponds to the consequence of the Anderson's theorem[20]. Figure 1 also shows that the Anderson's theorem is broken for the magnetic impurities (blue triangle). What is an important thing here is that the resultant properties are completely equivalent to those of the conventional s-wave superconductivity.

B. Pseudo-Scalar gap (odd-parity topological superconductivity)

Let us focus on the impurity effects of the pseudo-scalar gap (full-gap topological superconductivity). Firstly, we use the same mass and chemical potential as in Fig. 1, $(M_0, \mu) = (-0.6, 0.8)$ (i.e., $\beta \sim 0.88$). Thus, we study the impurity effects in a non-relativistic region. Figure 2 shows that both the non-magnetic (green square) and the magnetic (blue triangle) impurities induce in-gap states. The result for the non-magnetic impurities is similar to that in a two-dimensional s-wave

TABLE I. Summary of robustness against non-magnetic impurities, with different types of gap functions and β. The quantity β characterizes the weight of relativistic effects [See Eq. (6)]. When $\beta < 1$, the system is in non-relativistic regime, whereas when $\beta > 1$, the system is in relativistic regime. In the second column, according to Refs. 7 and 8, even parity indicates a non-topological state, while odd parity means a topological state. The fifth column shows the density of states without impurities at $E = 3\Delta$, to estimate normal-state contributions. The last column shows the corresponding figures.

Gap type	Parity	Relativity (β)	Robustness	Density of states (at $E = 3\Delta$)	Figure
scalar	even	0.88	robust	0.04	Figure 1
pseudo-scalar	odd	0.88	fragile	0.04	Figure 2
pseudo-scalar	odd	2.83	robust	0.008	Figure 3
pseudo-scalar	odd	2.83	robust	0.04	Figure 4

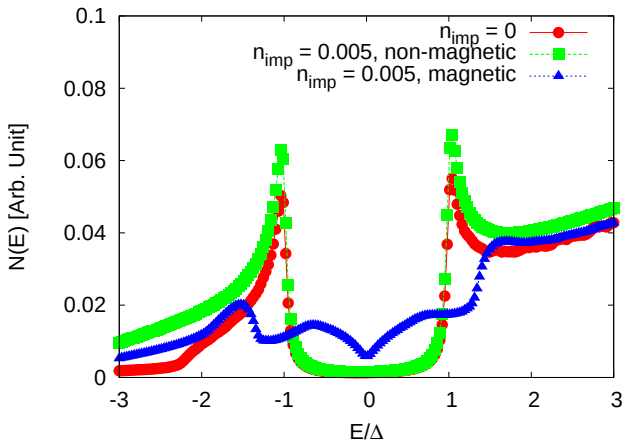

FIG. 1. (Color online) Energy dependence of the density of states $N(E)$ in the scalar gap (a non-topological superconductor), with different types of impurities. The red circle indicates the DOS without impurity scattering, whereas the green square and the blue triangle are the results for, respectively, non-magnetic and magnetic impurities. The horizontal axis is energy E/Δ, with superconducting gap amplitude $\Delta = 0.1$ eV.

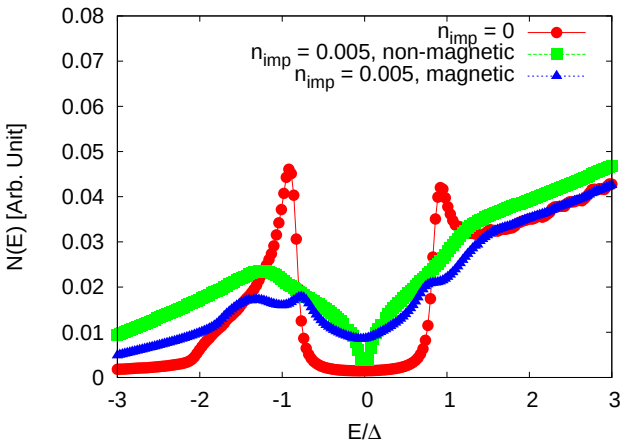

FIG. 2. (Color online) Energy dependence of the density of states $N(E)$ in a pseudo-scalar gap (an odd-parity topological superconductor) in a non-relativistic region ($\beta \sim 0.88$), with different types of impurities. The legends are the same as in Fig. 1. The horizontal axis is energy E/Δ, with superconducting gap amplitude $\Delta = 0.1$ eV.

topological superconductor.[25] In the adopted parameters, the topological fully-gapped superconductivity is fragile against non-magnetic impurities.

Secondly, we examine β-dependence of the robustness against non-magnetic impurities. We set $(M_0, \mu) = (-0.1, 0.3)$. It means that $\beta \sim 2.83$ (a relativistic region). Figure 3 shows that the non-magnetic impurities (green square) does not induce any in-gap state. This remarkable effect is quite similar to the case for the non-topological fully-gapped superconductivity (See Fig. 1). We note here that in a high energy domain (e.g., $E/\Delta \sim 3$) the DOS for the non-magnetic impurities is much different from the one without impurities, compared to Figs. 1 and 2. This originates from the fixed chemical potential and the resultant filling change.

Now, we show that in the pseudo-scalar-type topological superconductivity the robustness against non-magnetic impurities is predominated by the relativity indicator β. Figures 2 and 3 show that the DOS at $E = 3\Delta$ for $(M_0, \mu) = (-0.6, 0.8)$ (Fig. 2) is three times smaller than that for $(M_0, \mu) = (-0.1, 0.3)$ (Fig. 3). It indicates that the above calculations for a relativistic region are performed when the normal-state DOS is relatively small. Intuitively, this small normal-state DOS can be an alternative origin to reduce the effects of non-magnetic impurity scattering. To clarify the origin of the robustness, we examine a different model parameter set, $(\bar{D}_1, \bar{D}_2, \bar{B}_1, \bar{B}_2, \bar{A}_1, \bar{A}_2) = (0, 0, -0.5, -0.75, 1/3, 1.5/3)$ and $(M_0, \mu) = (-0.6, 0.8)$. The relativity indicator is $\beta \sim 2.83$ (a relativistic region). We find that the spin-orbit couplings are three times smaller than in the parameter set in Figs. 2 and 3. Figure 4 shows that the DOS at $E = 3\Delta$ is similar to Fig. 2. We stress that the robustness against non-magnetic impurities is the same as in the previous relativistic region (See Fig. 3). Therefore, we claim that the relativity indicator β characterizes well the robustness against non-magnetic impurities in the full-gap topological superconductivity.

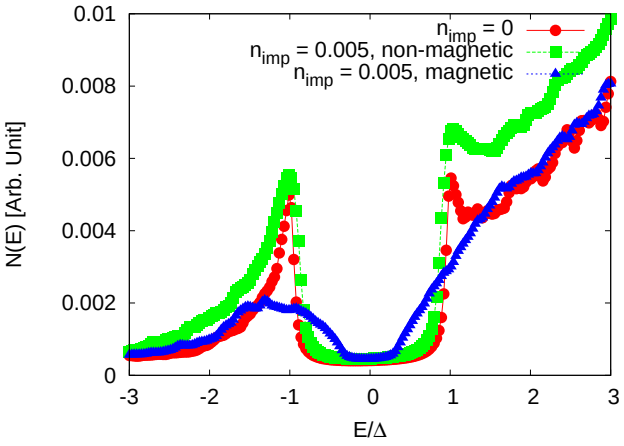

FIG. 3. (Color online) Energy dependence of the density of states $N(E)$ in a pseudo-scalar gap (an odd-parity topological superconductor) in a relativistic region ($\beta \sim 2.83$), with different types of impurities. The legends are the same as in Fig. 1. The horizontal axis is energy E/Δ, with superconducting gap amplitude $\Delta = 0.1$ eV.

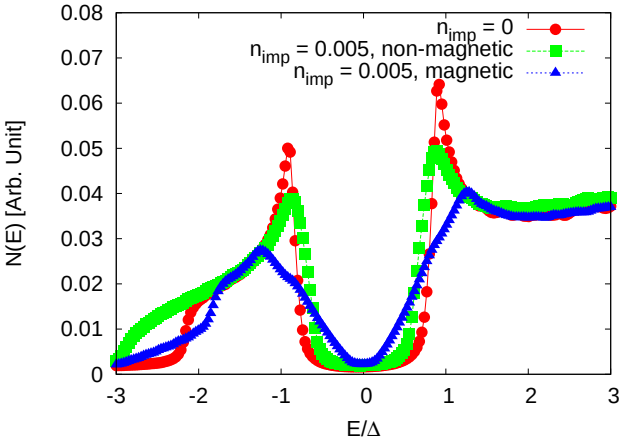

FIG. 4. (Color online) Energy dependence of the density of states $N(E)$ in a pseudo-scalar gap (an odd-parity topological superconductor) in a relativistic region ($\beta \sim 2.83$), with different types of impurities. The spin-orbit couplings are three times smaller than in Fig. 3. The legends are the same as in Fig. 1. The horizontal axis is energy E/Δ, with superconducting gap amplitude $\Delta = 0.1$ eV.

C. Unified picture of impurity effects with a relativistic effect

Now, we show deeper understanding of the present impurity effects, in terms of relativity. To see this point, we derive an effective BdG Hamiltonian in a clean case ($n_{\rm imp} = 0$), with either the non-relativistic limit ($\beta \to 0$) or the ultra-relativistic limit ($\beta \to \infty$). Since the relativity indicator β appears in a low-energy behavior in the normal-state Hamiltonian, we focus on linearized normal-state Hamiltonian (5). The 8×8 linearized BdG equations in the Dirac basis are

$$\begin{pmatrix} M_0 - \mu & \boldsymbol{k}' \cdot \boldsymbol{s} & \Delta^{11} & \Delta^{12} \\ \boldsymbol{k}' \cdot \boldsymbol{s} & -M_0 - \mu & \Delta^{21} & \Delta^{22} \\ \Delta^{11\dagger} & \Delta^{21\dagger} & -M_0 + \mu & \boldsymbol{k}' \cdot \boldsymbol{s}^* \\ \Delta^{12\dagger} & \Delta^{22\dagger} & \boldsymbol{k}' \cdot \boldsymbol{s}^* & M_0 + \mu \end{pmatrix} \boldsymbol{\phi} = E\boldsymbol{\phi}, \tag{13}$$

with ${}^{\rm t}\boldsymbol{\phi} = ({}^{\rm t}\boldsymbol{F}, {}^{\rm t}\boldsymbol{G}, {}^{\rm t}\boldsymbol{F}', {}^{\rm t}\boldsymbol{G}')$ and $\boldsymbol{k}' = (\bar{A}_2 k_x, \bar{A}_2 k_y, \bar{A}_1 k_z)$. We find that $\Delta^{11} = \Delta^{22} = i f^{\rm s} s^2$ and $\Delta^{12} = \Delta^{21} = i f^{\rm ps} s^2$.

1. *Non-relativistic limit*

We consider the non-relativistic limit ($\beta \to 0$). Since the relativity indicator β vanishes when $\mu = M_0$, we use another variable $\mu' = \mu - M_0$, for examining the non-relativistic case. The non-relativistic behaviors of the Dirac equation are obtained by expansion with respect to the order of $1/M_0$. In this approach[35], the upper two components of the Dirac spinor in the Dirac basis is regarded as large components, whereas the others are small ones. Precisely speaking, the large components correspond to the $+1$-eigenspace of γ^0 in the Dirac basis. Dropping parts relevant to the small components order by order, projection onto the large components is achieved. In the BdG equations, we consider $\boldsymbol{F}$ and $\boldsymbol{F}'$ to be the large components. Then, we perform inverse-mass expansion, under the condition that $E/|M_0| \ll 1$, $\mu'/|M_0| \ll 1$, and $\Delta/|M_0| \ll 1$. The resultant equations are given as

$$\begin{pmatrix} \frac{\boldsymbol{k}'^2}{2M_0} - \mu' & \Delta_{\rm eff}(\boldsymbol{k}') \\ \Delta^\dagger_{\rm eff}(\boldsymbol{k}') & -\frac{\boldsymbol{k}'^2}{2M_0} + \mu' \end{pmatrix} \begin{pmatrix} \boldsymbol{F} \\ \boldsymbol{F}' \end{pmatrix} = E \begin{pmatrix} \boldsymbol{F} \\ \boldsymbol{F}' \end{pmatrix}, \tag{14}$$

with

$$\Delta_{\rm eff}(\boldsymbol{k}') = \left[f^{\rm s} + \frac{f^{\rm ps}}{M_0} (\boldsymbol{k}' \cdot \boldsymbol{s}) \right] (is^2). \tag{15}$$

For even parity ($f^{\rm s} \neq 0$ and $f^{\rm ps} = 0$), the above equations are equivalent to the BdG equations of the s-wave superconductivity. This indicates that the non-topological fully-gapped superconductivity is regarded as the conventional s-wave superconductivity, in the non-relativistic limit. In contrast, when $f^{\rm s} = 0$ and $f^{\rm ps} \neq 0$ (odd parity), the effective gap function (15) is equivalent to a p-wave one. Therefore, the pseudo-scalar gap function in the non-relativistic limit is fragile against non-magnetic impurities, since the Anderson's theorem is not valid in the p-wave superconductivity. This p-wave like behavior is consistent with the results by a quasi-classical approach[31]. Two of the authors (YN and MM) showed that the pseudo-scalar gap is equivalent to the spin-triplet order parameter, within the quasi-classical approximation. In the spin-triplet order parameter, the $\boldsymbol{d}$-vector rotates

in momentum space (i.e., $\boldsymbol{d}(\boldsymbol{k}) \propto \boldsymbol{k}$). Therefore, the superconductivity is broken significantly via impurity scattering. The induced DOS in the low energy region shown in Fig. 2 can be explained by this correspondence.

2. Ultra-relativistic limit

We study the ultra-relativistic limit ($\beta \to \infty$). We use the Weyl basis, since the normal-state Hamiltonian with $\beta \to \infty$ corresponds to the massless Dirac equation (the Weyl equation). The chirarity (i.e., the eigenvalues of γ^5) is good quantum number when $M_0 \to 0$. Thus, in the Weyl basis γ^5 is a diagonal form (in the Dirac basis γ^0 is diagonal). We will use over-line symbol to specify the quantities in the Weyl basis. The linearized BdG equations are

$$\begin{pmatrix} \bar{h}_0(\boldsymbol{k}') & \bar{\Delta}_{\rm pair} \\ \bar{\Delta}^\dagger_{\rm pair} & -\bar{h}_0^*(-\boldsymbol{k}') \end{pmatrix} \bar{\boldsymbol{\phi}} = E\bar{\boldsymbol{\phi}}, \tag{16}$$

with

$$\bar{h}_0 = \begin{pmatrix} -\boldsymbol{k}'\cdot\boldsymbol{s} - \mu & M_0 \\ M_0 & \boldsymbol{k}'\cdot\boldsymbol{s} - \mu \end{pmatrix}, \tag{17}$$

and ${}^t\bar{\boldsymbol{\phi}} = ({}^t\bar{\boldsymbol{F}}, {}^t\bar{\boldsymbol{G}}, {}^t\bar{\boldsymbol{F}}', {}^t\bar{\boldsymbol{G}}')$. The 4×4 pairing potential matrix including the scalar and the pseudo-scalar gaps is

$$\bar{\Delta}_{\rm pair} = f^{\rm s}\begin{pmatrix} is^2 & 0 \\ 0 & is^2 \end{pmatrix} + f^{\rm ps}\begin{pmatrix} -is^2 & 0 \\ 0 & is^2 \end{pmatrix}. \tag{18}$$

Taking $M_0 \to 0$, we find that the BdG equations are divided into a left-handed sector ($\bar{\boldsymbol{G}}$ and $\bar{\boldsymbol{G}}'$) and a right-handed sector ($\bar{\boldsymbol{F}}$ and $\bar{\boldsymbol{F}}'$), for both the scalar and the pseudo-scalar gaps. As for $\bar{\boldsymbol{G}}$ and $\bar{\boldsymbol{G}}'$, we have

$$\begin{pmatrix} \boldsymbol{k}'\cdot\boldsymbol{s} - \mu & is^2 f^{\rm s(ps)} \\ -is^2 f^{\rm s(ps)\,*} & \boldsymbol{k}'\cdot\boldsymbol{s}^* + \mu \end{pmatrix} \begin{pmatrix} \bar{\boldsymbol{G}} \\ \bar{\boldsymbol{G}}' \end{pmatrix} = E \begin{pmatrix} \bar{\boldsymbol{G}} \\ \bar{\boldsymbol{G}}' \end{pmatrix}. \tag{19}$$

We can find the same expression for $\bar{\boldsymbol{F}}$ and $\bar{\boldsymbol{F}}'$, except for the sign factor in each block. Remarkably, both the scalar and the pseudo-scalar effective gap functions are equivalent to the s-wave gap function. Furthermore, we find that non-magnetic potential (8) and magnetic impurity potentials (9) are decoupled between the left-handed and the right-handed sectors in the Weyl basis. These results indicate that the present model in the ultra-relativistic limit has a robust feature against non-magnetic impurities associated with the Anderson's theorem, irrelevant with the parity.

IV. SUMMARY

In conclusion, we calculated the density of states and examined the presence of in-gap states in the three-dimensional topological superconductors described by the massive Dirac Hamiltonian, using a self-consistent T-matrix approach. We found that the results are summarized well by the material variable β, which characterize relativistic effects in h_0. In non-relativistic region, we find that the Anderson's theorem (i.e., the robustness against non-magnetic impurities) is violated, since a p-wave character involved in the topological superconducting order is predominant. In ultra-relativistic region, the effective Hamiltonian is the same as the s-wave Hamiltonian, irrespective of the gap-function types. Therefore, we claim that a three-dimensional topological superconductor with time-reversal symmetry and s-wave on-site pairing has either p- or s-wave characters, depending on the relativistic effects in the normal-state Hamiltonian.

ACKNOWLEDGEMENTS

We thank H. Nakamura for helpful discussions and comments. The calculations were performed using the supercomputing system PRIMERGY BX900 at the Japan Atomic Energy Agency. This study has been supported by Grants-in-Aid for Scientific Research from the Ministry of Education, Culture, Sports, Science and Technology of Japan.

[1] *The Quantum Hall Effect*, 2nd ed. edited by R. E. Prange and S. M. Girvin (Springer-Verlag, New York, 1990).
[2] M. Nakahara, *Geometry, Topology and Physics*, 2nd ed. (CRC Press, Boca Raton, London and New York, 2003).
[3] G. E. Volovik, *The Universe in a Helium Droplet* (Oxford University Press, New York, 2003).
[4] M. Z. Hasan and C. L. Kane, Rev. Mod. Phys. **82**, 3045 (2010).
[5] Y. Ando, J. Phys. Soc. Jpn. **82** 102001 (2013).
[6] A. P. Schnyder, S. Ryu, A. Furusaki, and A. W. W. Ludwig, Phys. Rev. B **78**, 195125 (2008).
[7] L. Fu and E. Berg, Phys. Rev. Lett. **105**, 097001 (2010).
[8] M. Sato, Phys. Rev. B **81**, 220504(R) (2010).
[9] M. Sato, Y. Takahashi, and S. Fujimoto, Phys. Rev. B **82**, 134521 (2010).
[10] D. J. Thouless, M. Kohmoto, M. P. Nightingale, and M. den Nijs, Phys. Rev. Lett. **49**, 405 (1982).
[11] C. L. Kane and E. J. Mele, Phys. Rev. Lett. **95**, 146802 (2005).
[12] L. Fu and C. L. Kane, Phys. Rev. B **76**, 045302 (2007).
[13] Y. S. Hor, A. J. Williams, J. G. Checkelsky, P. Roushan, J. Seo, Q. Xu, H. W. Zandbergen, A. Yazdani, N. P. Ong, and R. J. Cava, Phys. Rev. Lett. **104**, 057001 (2010).
[14] L. A. Wray, S.-Y. Xu, Y. Xia, Y. S. Hor, D. Qian, A. V. Fedorov, H. Lin, A. Bansil, R. J. Cava, and M. Z. Hasan, Nature Phys. **6**, 855 (2010).

[15] S. Sasaki, M. Kriener, K. Segawa, K. Yada, Y. Tanaka, M. Sato, and Y. Ando, Phys. Rev. Lett. **107**, 217001 (2011).

[16] T. Kirzhner, E. Lahoud, K. B. Chaska, Z. Salman, and A. Kanigel, Phys. Rev. B **86**, 064517 (2012).

[17] P. Das, Y. Suzuki, M. Tachiki, and K. Kadowaki, Phys. Rev. B **83**, 220513(R) (2011).

[18] N. Levy, T. Zhang, J. Ha, F. Sharifi, A. Alec Talin, Y. Kuk, and J. A. Stroscio, Phys. Rev. Lett. **110**, 117001 (2013).

[19] Y. Nishida, Phys. Rev. D **81** 074004 (2010).

[20] N. B. Kopnin, *Theory of Nonequilibrium Superconductivity* (Oxford University Press, New York, 2001).

[21] P. Hirschfeld, D. Vollhardt, and P. Wölfle, Solid State Commun **59**, 111 (1986).

[22] S. Schmitt–Rink, K. Miyake, and C. M. Varma, Phys. Rev. Lett. **57**, 2575 (1986).

[23] T. Hotta, J. Phys. Soc. Jpn. **62**, 274 (1993).

[24] G. Preosti and P. Muzikar, Phys. Rev. B **54**, 3489 (1996).

[25] Y. Nagai, Y. Ota, and M. Machida, arXiv:1312.3065 (unpublished).

[26] L. Hao and T. K. Lee, Phys. Rev. B **83**, 134516 (2011).

[27] A. Yamakage, K. Yada, M. Sato, and Y. Tanaka, Phys. Rev. B **85**, 180509 (2012).

[28] Y. Nagai, H. Nakamura, and M. Machida, Phys. Rev. B **86**, 094507 (2012).

[29] T. Mizushima, A. Yamakage, M. Sato, and Yukio Tanaka, arXiv:1311.2768 (unpublished).

[30] Y. Nagai, H. Nakamura, and M. Machida, arXiv:1211.0125 to be published in J. Phys. Soc. Jpn.

[31] Y. Nagai, H. Nakamura, and M. Machida, arXiv:1305.3025, to be published in J. Phys. Soc. Jpn.

[32] A. M. Black-Schaffer and A. V. Balatsky, Phys. Rev. B **87**, 220506(R) (2013).

[33] P. Goswami and B. Roy, arXiv:1211.4023.

[34] H. Zhang, C.-X. Liu, X.-L. Qi, X. Dai, Z. Fang, and S.-C. Zhang, Nature Phys. **5**, 438 (2009).

[35] C. Itzykson and J.-B. Zuber, *Quantum Field Theory* (Dover, New York, 2005).

[36] J. L. van Hemmen, Z. Phys. B **38**, 271 (1980).

[37] Hao and Lee[26] use a different choice for the spatial inversion. The present expressions can be related to their formulae, via a map $\sigma^3 \to \sigma^1$.

[38] We consider that this indicator only depends on $\bar{A}_2$, not $\bar{A}_1$, since the in-plane spin-orbit coupling $\bar{A}_2$ is always larger than the inter-plane spin-orbit coupling A_1.

[39] G. P. Mahan, *Many-Particle Physics*, 3rd ed. (Springer-Verlag, Berlin Heidelberg, 2000) Chap.4.